

PRD Draft v3.0
Authors: M. Martinez
(IFAE-Barcelona)

Study of Jet Shapes in Inclusive Jet Production at the Tevatron
(The CDF II Collaboration)

We report on a study of jet shapes in inclusive jet production in $p\bar{p}$ collisions at $\sqrt{s} = 1.96$ TeV using the CDF II detector. Jets are reconstructed using the midpoint algorithm. Measurements are performed at the hadron level for jets with rapidity $0.1 < |Y^{\text{jet}}| < 0.7$ and transverse momentum $37 \text{ GeV} < P_T^{\text{jet}} < 380 \text{ GeV}$. The measured jet shapes are compared to predictions from several leading-order QCD parton-shower Monte Carlo programs.

PACS numbers: Need PACS numbers

I. INTRODUCTION

The internal structure of jets is dominated by multi-gluon emissions from the primary final-state parton. It is sensitive to the relative quark- and gluon-jet fraction and receives contributions from soft-gluon initial-state radiation and beam remnant-remnant interactions. The study of jet shapes at the Tevatron provides a stringent test of QCD predictions and tests the validity of the models for parton cascades and soft-gluon emissions in hadron-hadron collisions. Measurements of the jet shape have been performed in $p\bar{p}$ collisions at $\sqrt{s} = 1.8$ TeV [1], deeply inelastic scattering [2] and photoproduction [3] processes in $e^\pm p$ collisions at HERA, and e^+e^- interactions at LEP1 [4]. In this letter, jet shapes in $p\bar{p}$ collisions at $\sqrt{s} = 1.96$ TeV are studied at the hadron level in a wide range in jet transverse momentum.

II. EXPERIMENTAL SETUP

The CDF II detector is described in detail in [5]. In the following section, the sub-detectors most relevant for this analysis are shortly discussed. The detector has a charged particle tracking system immersed in a 1.4 T magnetic field, aligned coaxially with the beam line. A silicon microstrip detector provides tracking over the radial range 1.35 to 28 cm. A 3.1 m long open-cell drift chamber, the Central Outer Tracked (COT), covers the radial range from 44 to 132 cm. The fiducial region of the silicon detector extends to $|\eta| \sim 2$ [6], while the COT provides coverage for $|\eta| \leq 1$. Segmented electromagnetic and hadronic sampling calorimeters (CAL), arranged in a projective tower geometry, surround the tracking system and measure the energy flow of interacting particles in the pseudorapidity range $|\eta| \leq 3.6$. Cerenkov counters located in the $3.7 < |\eta| < 4.7$ region [7] measure the average number of inelastic $p\bar{p}$ collisions per bunch crossing and thereby determine the beam luminosity. A three-level trigger system is used to select events online.

III. MONTE CARLO SIMULATION

Monte Carlo (MC) event samples are used to determine the response of the detector and the correction factors for the measured jet shapes. Samples of simulated inclusive jet events have been generated using the PYTHIA 6.203 [8] and HERWIG 6.4 [9] MC generators. In both programs, the partonic interactions are generated using leading-order QCD matrix elements, including initial and final parton showers. CTEQ5L [10] parton distribution functions are used for the proton and antiproton. The PYTHIA samples have been created using a special tuned set of parameters (denoted as PYTHIA-Tune A [11]) that control soft-gluon emissions in the final state. Tune A was determined as a result of dedicated studies of the underlying event performed using CDF Run I data [12]. In addition, two different PYTHIA samples have been generated using default parameters with and without the contribution from multiple parton interactions (MPI) between proton and antiproton remnants, the latter denoted as PYTHIA-(no MPI). Fragmentation into hadrons is carried out using the string model [13] as implemented in JETSET [14] in the case of PYTHIA and the cluster model [15] in HERWIG. The generated samples are passed through the CDF detector simulation, and then reconstructed and analyzed using the same analysis chain as in the data.

IV. JET RECONSTRUCTION

An iterative cone-based midpoint algorithm [16] in the $Y - \phi$ plane with cone radius $R = 0.7$ is used to reconstruct jets from the energy deposits in the CAL towers for both data and MC simulated events and from final-state particles for MC generated events. Overlapping jets are merged if their shared momentum is larger than 75% [17] of the jet with smaller transverse momentum, otherwise two jets are formed and the common CAL towers or final-state hadrons are assigned to the nearest jet. The reconstruction of jets in the CAL is studied using MC event samples. These studies indicate that the direction of the jet, $Y_{\text{CAL}}^{\text{jet}}$ and $\phi_{\text{CAL}}^{\text{jet}}$, is well reconstructed in the detector. The jet transverse momentum, $P_{T,\text{CAL}}^{\text{jet}}$, is systematically underestimated by about 20% at low $P_{T,\text{CAL}}^{\text{jet}}$ and by 10% at very high $P_{T,\text{CAL}}^{\text{jet}}$. It is reconstructed with a resolution of about

20% at low $P_{T,\text{CAL}}^{\text{jet}}$ which improves as the jet transverse momentum increases. This is mainly due to the non-compensating nature of the CAL. An average correction is extracted from the MC using the following procedure: matched pairs of jets ($Y - \phi$ plane) are used to study the difference between the jet transverse momentum at the hadron level, $P_{T,\text{HAD}}^{\text{jet}}$, and the corresponding measurement in the calorimeter, $P_{T,\text{CAL}}^{\text{jet}}$. The resulting correlation is used to extract multiplicative correction factors, $C(P_{T,\text{CAL}}^{\text{jet}})$, which are then applied to the measured jets to obtain the corrected jet transverse momenta, $P_{T,\text{COR}}^{\text{jet}}$.

V. EVENT SELECTION

This analysis is based on a sample of inclusive jet events selected from the CDF Run II data corresponding to a total integrated luminosity of 170 pb^{-1} . Events were collected online using a three-level trigger based on the measured energy deposits in the CAL towers. In the third-level trigger, jets are reconstructed using the CDF Run I cone algorithm [1] with several different thresholds on the measured jet transverse energy. Offline, jets are reconstructed using the midpoint algorithm, as explained above, starting from seed calorimeter towers with transverse momentum above 1 GeV and only considering towers with a minimum transverse momentum of 100 MeV in the clustering procedure. The following selection criteria have been imposed:

- One and only one reconstructed primary vertex with z-component, V_Z , in the region $|V_Z| < 60 \text{ cm}$. Events with more than one primary vertex are removed to eliminate contributions from pile-up events with multiple proton-antiproton interactions per beam crossing.
- $\cancel{E}_T/\sqrt{E_T} < 3.5 \text{ GeV}^{-1/2}$, where \cancel{E}_T (E_T) denotes the missing (total) transverse energy of the event as determined from the energy deposits in the calorimeter towers. This cut eliminates contributions from beam-related backgrounds and cosmic rays.
- At least one jet with $P_{T,\text{COR}}^{\text{jet}} > 37 \text{ GeV}$ (see previous section) and Y^{jet} in the region $0.1 < |Y^{\text{jet}}| < 0.7$.

For each data sample, the thresholds on the uncorrected $P_{T,\text{CAL}}$ have been selected such that the trigger is fully efficient in the whole kinematic region under study.

VI. JET SHAPE

A. Jet shape definition

The differential jet shape, $\rho(r)$, is defined as the average fraction of the jet transverse momentum that lies inside an annulus of inner radius $r - \delta r/2$ and outer radius $r + \delta r/2$ around the jet axis:

$$\rho(r) = \frac{1}{\delta r} \frac{1}{N_{\text{jet}}} \sum_{\text{jets}} \frac{P_T(r - \delta r/2, r + \delta r/2)}{P_T(0, R)}, \quad 0 \leq r \leq R \quad (1)$$

where N_{jet} denotes the number of jets, $P_T(r - \delta r/2, r + \delta r/2)$ is the transverse momentum within an annulus and the jet shape is determined for values of r between 0.05 and 0.65 using $\delta r = 0.1$ intervals.

Similarly, the integrated jet shape, $\Psi(r)$, is defined as the average fraction of the jet transverse momentum that lies inside a cone of radius r concentric to the jet cone:

$$\Psi(r) = \frac{1}{N_{\text{jet}}} \sum_{\text{jets}} \frac{P_T(0, r)}{P_T(0, R)}, \quad 0 \leq r \leq R \quad (2)$$

where, by definition, $\Psi(r = R) = 1$. The integrated jet shape is determined in intervals $\delta r = 0.1$ between $r = 0$ and $r = 0.7$.

B. Jet shape reconstruction

Calorimeter towers are used for both data and MC simulated events to reconstruct the differential jet shape. For each jet, the scalar sum of the transverse momentum of the CAL towers assigned to it, $P_T(r-\delta r/2, r+\delta r/2)$, with a distance to the jet axis $r' = \sqrt{\delta Y^2 + \delta\phi^2}$ between $r - \delta r/2$ and $r + \delta r/2$, is determined and divided by $P_T(0, R)$. The differential jet shape, $\rho_{\text{MC}}^{\text{CAL}}(r)$, is then determined following the prescription in Eq. 1. Similarly, the integrated jet shape, $\Psi_{\text{MC}}^{\text{CAL}}(r)$, is reconstructed using the CAL towers as defined in Eq. 2. The same procedure is applied to the final-state particles in MC generated events to reconstruct the differential and integrated jet shapes at the hadron level, $\rho_{\text{MC}}^{\text{HAD}}(r)$ and $\Psi_{\text{MC}}^{\text{HAD}}(r)$, respectively.

C. Jet shape using charged particles

The CDF tracking system provides an alternative method to measure the shape of the jets using charged particles. For each jet, tracks with transverse momentum, p_T^{track} , above 0.5 GeV and pseudorapidity, η^{track} , in the region $|\eta^{\text{track}}| < 1.5$ are assigned to it if their distances with respect to the jet axis, $r = \sqrt{(Y^{\text{jet}} - \eta^{\text{track}})^2 + (\phi^{\text{jet}} - \phi^{\text{track}})^2}$, are smaller than 0.7, and the projected z-vertices of the tracks are within 2 cm around the z-position of the primary vertex. The differential and integrated jet shapes, $\rho^{\text{TRKS}}(r)$ and $\Psi^{\text{TRKS}}(r)$, are reconstructed following Eqs. 1 and 2 where the tracks assigned to each jet are used. Detailed studies have been performed on track reconstruction efficiency inside jets as a function of r and the jet and track transverse momenta. The difference between efficiencies in the data and MC are typically smaller than 3% and approximately independent of r for tracks with $0.5 < p_T^{\text{track}} < 2.0$ GeV. For tracks with $p_T^{\text{track}} > 2.0$ GeV, the difference in efficiency is of the order of 5% at the core of the jet, and it decreases as r increases up to $r = 0.5$ from where no difference is observed. The effect on the reconstructed jet shapes is smaller than 0.5% and thus has been absorbed into the systematic error. The measured jet shapes using tracks are consistent with those using CAL towers and have been employed to study systematic uncertainties on the central measurements (see next section).

VII. UNFOLDING AND SYSTEMATIC STUDIES

The measured jet shapes, as determined using CAL towers, are corrected back to the hadron level using MC samples of generated events. PYTHIA-Tune A provides a good description of the measured jet shapes in all regions of P_T^{jet} and is used to determine the correction factors in the unfolding procedure. The corrected differential and integrated jet shapes, $\rho(r)$ and $\Psi(r)$, refer to midpoint jets at the hadron level with cone size $R = 0.7$ in the region $0.1 < |Y^{\text{jet}}| < 0.7$ and $37 \text{ GeV} < P_T^{\text{jet}} < 380 \text{ GeV}$.

A. Jet shape correction

The measured jet shapes are corrected for acceptance and smearing effects back to the hadron level. The correction factors also account for the efficiency of the selection criteria and for jet reconstruction in the calorimeter. Differential and integrated jet shapes are reconstructed with MC samples using both CAL towers, $\rho_{\text{MC}}^{\text{CAL}}(r)$ and $\Psi_{\text{MC}}^{\text{CAL}}(r)$, and final-state hadrons, $\rho_{\text{MC}}^{\text{HAD}}(r)$ and $\Psi_{\text{MC}}^{\text{HAD}}(r)$, in different regions of $P_{T,\text{COR}}^{\text{jet}}$ and $P_{T,\text{HAD}}^{\text{jet}}$, respectively. Correction factors, defined as $D(r) = \rho_{\text{MC}}^{\text{HAD}}(r)/\rho_{\text{MC}}^{\text{CAL}}(r)$ and $I(r) = \Psi_{\text{MC}}^{\text{HAD}}(r)/\Psi_{\text{MC}}^{\text{CAL}}(r)$, are then computed separately in each bin of $P_{T,\text{COR}}^{\text{jet}}$. The corrected differential and integrated measurements are determined from the measured jet shapes as $\rho(r) = D(r) \cdot \rho_{\text{MC}}^{\text{CAL}}(r)$ and $\Psi(r) = I(r) \cdot \Psi_{\text{MC}}^{\text{CAL}}(r)$. The correction factors $D(r)$ do not show a significant dependence on $P_{T,\text{COR}}^{\text{jet}}$ and vary between 0.9 and 1.2 as r increases. For the integrated jet shapes, the correction factors $I(r)$ differ from unity by less than 10% for $r > 0.2$.

B. Systematic uncertainties

A detailed study of the different sources of systematic uncertainties on the measured jet shapes has been performed:

- The measured jet transverse momentum has been varied by $\pm 5\%$ in the data to account for the uncertainty on the determination of the absolute energy scale in the calorimeter. The effect on the measured jet shapes is less than 2%.
- The unfolding procedure has been repeated using bin-by-bin correction factors extracted from HERWIG instead of PYTHIA-Tune A to account for any possible dependence on the modeling of parton cascades. The effect on the measured jet shapes is typically below 5%.
- The ratio of uncorrected jet shape measurements, as determined using CAL towers and tracks, $\rho^{\text{CAL}}(r)/\rho^{\text{TRKS}}(r)$ and $\Psi^{\text{CAL}}(r)/\Psi^{\text{TRKS}}(r)$, are compared between data and MC simulated events. Any deviation from unity in the data/MC double ratio is included in the systematic error to account for the uncertainty on the description of the inactive material in front of the calorimeter and its response to low-energy particles. The effect on the measured jet shapes is typically below 5%.
- The measurements are performed in different regions of Tevatron instantaneous luminosity (between $2 \cdot 10^{30} \text{ cm}^{-2}\text{s}^{-1}$ and $40 \cdot 10^{30} \text{ cm}^{-2}\text{s}^{-1}$) to account for possible remaining contributions from pile-up events. No significant effect is found.

The total systematic uncertainties on $\rho(r)$ and $\Psi(r)$ have been computed for the different r ranges by adding in quadrature the deviations from the central values. The statistical uncertainties are negligible compared to the systematic errors except for jets with $P_T^{\text{jet}} > 300 \text{ GeV}$ for which the measurements are dominated by statistical fluctuations. The systematic uncertainties have been added in quadrature to the statistical errors and the total uncertainties are shown in the figures.

VIII. RESULTS

A. Comparison with Monte Carlo

Figures 1 and 2 show the measured differential jet shapes, $\rho(r/R)$, as a function of P_T^{jet} for jets in the region $0.1 < |Y^{\text{jet}}| < 0.7$ and $37 \text{ GeV} < P_T^{\text{jet}} < 380 \text{ GeV}$, compared to PYTHIA-Tune A and HERWIG MC predictions. The measured jet shapes show a prominent peak at low r which indicates that the majority of the jet is concentrated at $r/R < 0.2$. At low P_T^{jet} , the fraction of transverse momentum at the core of the jet is about a factor of 60 times larger than that at the tail. This factor increases at higher P_T^{jet} indicating that jets become narrower with increasing jet transverse momentum. PYTHIA-Tune A provides a reasonable description of the measured jet shapes in all regions of P_T^{jet} . The jets predicted by HERWIG MC follow the measurements for $P_T^{\text{jet}} > 55 \text{ GeV}$ but tend to be narrower than the data at lower P_T^{jet} . This can be attributed to the different modeling of the contributions from soft-gluon radiations and remnant-remnant interactions in HERWIG, which are particularly important at low P_T^{jet} .

Figures 3 and 4 present the measured integrated jet shapes, $\Psi(r/R)$, as a function of P_T^{jet} , for jets with $0.1 < |Y^{\text{jet}}| < 0.7$ and $37 < P_T^{\text{jet}} < 380 \text{ GeV}$, compared to HERWIG, PYTHIA-Tune A, PYTHIA and PYTHIA-(no MPI) predictions, to illustrate the importance of a proper modeling of soft-gluon radiation in describing the measured jet shapes. In addition, Figure 5 shows, for a fixed radius $r_0 = 0.3$, the average fraction of the jet transverse momentum outside $r = r_0$, $1 - \Psi(r_0/R)$, as a function of P_T^{jet} where the points are located at the weighted mean in each P_T^{jet} range. The measurements show that the fraction of jet transverse momentum at a given fixed r_0/R increases ($1 - \Psi(r_0/R)$ decreases) with P_T^{jet} , indicating, as in the case of the differential measurements, that the jets become narrower as P_T^{jet} increases. PYTHIA with default parameters produces jets systematically narrower than the data in the whole region in P_T^{jet} . The contribution from secondary parton interactions between remnants to the predicted jet shapes (as shown by the difference

between PYTHIA and PYTHIA-(no MPI) predictions) is relatively small and decreases as P_T^{jet} increases. PYTHIA-Tune A predictions, which include an enhanced contribution from initial-state soft gluon radiation and a tuned set of parameter to control secondary parton interactions [11], describe all of the data well. HERWIG predictions describe the measured jet shapes well for $P_T^{\text{jet}} > 55 \text{ GeV}$.

B. Quark- and gluon-jet contributions

Figures 6 and 7 present the measured integrated jet shapes, $\Psi(r/R)$, as a function of P_T^{jet} , for jets with $0.1 < |Y^{\text{jet}}| < 0.7$ and $37 < P_T^{\text{jet}} < 380 \text{ GeV}$, compared to PYTHIA-Tune A predictions. The predictions are also shown separately for quark- and gluon-jets. Each hadron-level jet from PYTHIA is classified as a quark- or gluon-jet by matching ($Y - \phi$ plane) its directions with that of one of the outgoing partons from the hard interaction. The MC predictions indicate that the measured jet shapes are dominated by contributions from gluon-initiated jets at low P_T^{jet} while contributions from quark-initiated jets become important at high P_T^{jet} . This can be explained in terms of the different partonic contents in the proton and antiproton in the low- and high- P_T^{jet} regions, since the mixture of gluon- and quark-jet in the final state partially reflects the nature of the incoming partons that participate in the hard interaction.

Figure 8 shows the measured $1 - \Psi(r_0/R)$, $r_0 = 0.3$, as a function of P_T^{jet} compared to PYTHIA-Tune A predictions with quark- and gluon-jets shown separately. For a given type of parton-jet in the MC (quark- or gluon-jet), the observed trend with P_T^{jet} shows the running of the strong coupling constant, $\alpha_s(P_T^{\text{jet}})$. Hence, the value of the strong coupling constant, $\alpha_s(M_Z)$, could be determined from the evolution of the measured jet shapes as a function of P_T^{jet} .

IX. SUMMARY AND CONCLUSIONS

Jet shapes have been measured in inclusive jet production for jets in the kinematic region $37 \text{ GeV} < P_T^{\text{jet}} < 380 \text{ GeV}$ and $0.1 < |Y^{\text{jet}}| < 0.7$. Jets become narrower as P_T^{jet} increases, and the measured jet shapes show a strong dependence on the given gluon- and quark-jet content in the final state. PYTHIA MC predictions, using default parameters, do not describe the measured jet shapes in the entire P_T^{jet} range. PYTHIA-Tune A, which includes enhanced contributions from initial-state gluon radiation and secondary parton interactions between remnants, describe the data better. HERWIG gives a reasonable description of the measured jet shapes for jets with $P_T^{\text{jet}} > 55 \text{ GeV}$ but produces jets that are too narrow at lower P_T^{jet} . Jet shape measurements thus introduce strong constraints on phenomenological models describing soft-gluon radiation and the underlying event in hadron-hadron interactions.

Acknowledgments

We thank the Fermilab staff and the technical staffs of the participating institutions for their vital contributions. This work was supported by the U.S. Department of Energy and National Science Foundation; the Italian Istituto Nazionale di Fisica Nucleare; the Ministry of Education, Culture, Sports, Science and Technology of Japan; the Natural Sciences and Engineering Research Council of Canada; the National Science Council of the Republic of China; the Swiss National Science Foundation; the A.P. Sloan Foundation; the Bundesministerium fuer Bildung und Forschung, Germany; the Korean Science and Engineering Foundation and the Korean Research Foundation; the Particle Physics and Astronomy Research Council and the Royal Society, UK; the Russian Foundation for Basic Research; the Comision Interministerial de Ciencia y Tecnologia, Spain; and in part by the European Community's Human Potential Programme under contract

HPRN-CT-20002, Probe for New Physics.

- [1] CDF Collab., F. Abe et al., Phys. Rev. Lett. 70 (1993) 713.
D0 Collab., S. Abachi et al., Phys. Lett. B357 (1995) 500.
- [2] ZEUS Collab., J.Breitweg et al., The Eur. Phys. Journal C8 (1999) 3, 367-380.
H1 Collab., C. Adloff et al., Nucl. Phys. B545 (1999) 3-20.
- [3] ZEUS Collab., J.Breitweg et al., The Eur. Phys. Journal C2 (1998) 1, 61-75.
- [4] OPAL Collab., R. Akers et al., Zeit. f. Phys. C63 (1994) 197.
- [5] CDF II Collab., FERMILAB-PUB-96/390-E (1996).
- [6] The pseudorapidity is defined as $\eta = -\ln(\tan(\frac{\theta}{2}))$, where the polar angle θ is taken with respect to the proton beam direction. The rapidity is defined as $Y = \frac{1}{2}\ln(\frac{E+p_z}{E-p_z})$, where E denotes the energy and p_z is the component of the momentum along the proton beam direction.
- [7] D. Acosta et al., Nucl. Instrum. Meth. A 461, (2001) 540.
- [8] H.-U. Bengtsson and T. Sjöstrand, Comp. Phys. Comm. 46 (1987) 43.
- [9] G. Marchesini et al., Comp. Phys. Comm. 67 (1992) 465.
- [10] J. Pumplin et al., JHEP 0207 (2002) 012.
- [11] PYTHIA-Tune A MC samples are generated using the following tuned parameters in PYTHIA: PARP(67) = 4.0, MSTP(82) = 4, PARP(82) = 2.0, PARP(84) = 0.4, PARP(85) = 0.9, PARP(86) = 0.95, PARP(89) = 1800.0, PARP(90) = 0.25.
- [12] D. Acosta et al., CDF Collaboration, Phys. Rev. D65, 092002, (2002).
- [13] B. Andersson et al., Phys. Rep. 97 (1983) 31.
- [14] T. Sjöstrand, Comp. Phys. Comm. 39 (1986) 347.
- [15] B.R. Webber, Nucl. Phys. B 238 (1984) 492.
- [16] G. C. Blazey, et al., hep-ex/0005012.
S.D. Ellis, J. Huston and M. Toennesmann, hep-ph/0111434.
- [17] A 75% fraction (instead of the default 50% defined in the midpoint algorithm) has been used for easier comparison with measurements performed using the Run I CDF cone algorithm.

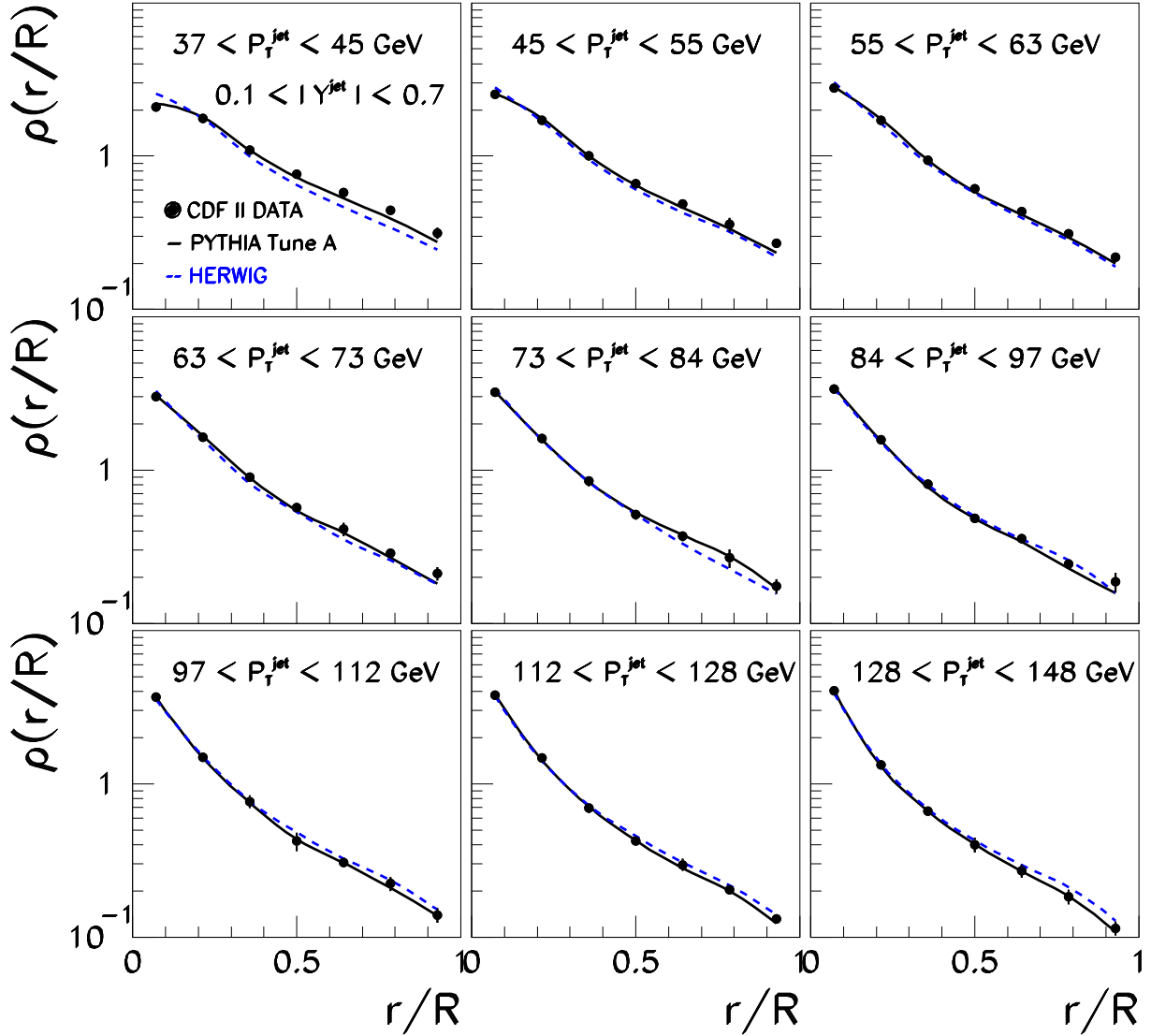


FIG. 1: The measured differential jet shape, $\rho(r/R)$, in inclusive jet production for jets with $0.1 < |Y^{\text{jet}}| < 0.7$ and $37 \text{ GeV} < P_T^{\text{jet}} < 148 \text{ GeV}$, is shown in different P_T^{jet} regions (back dots). Error bars indicate the statistical and systematic uncertainties added in quadrature. The predictions of PYTHIA-Tune A (solid lines) and HERWIG (dashed lines) are shown for comparison.

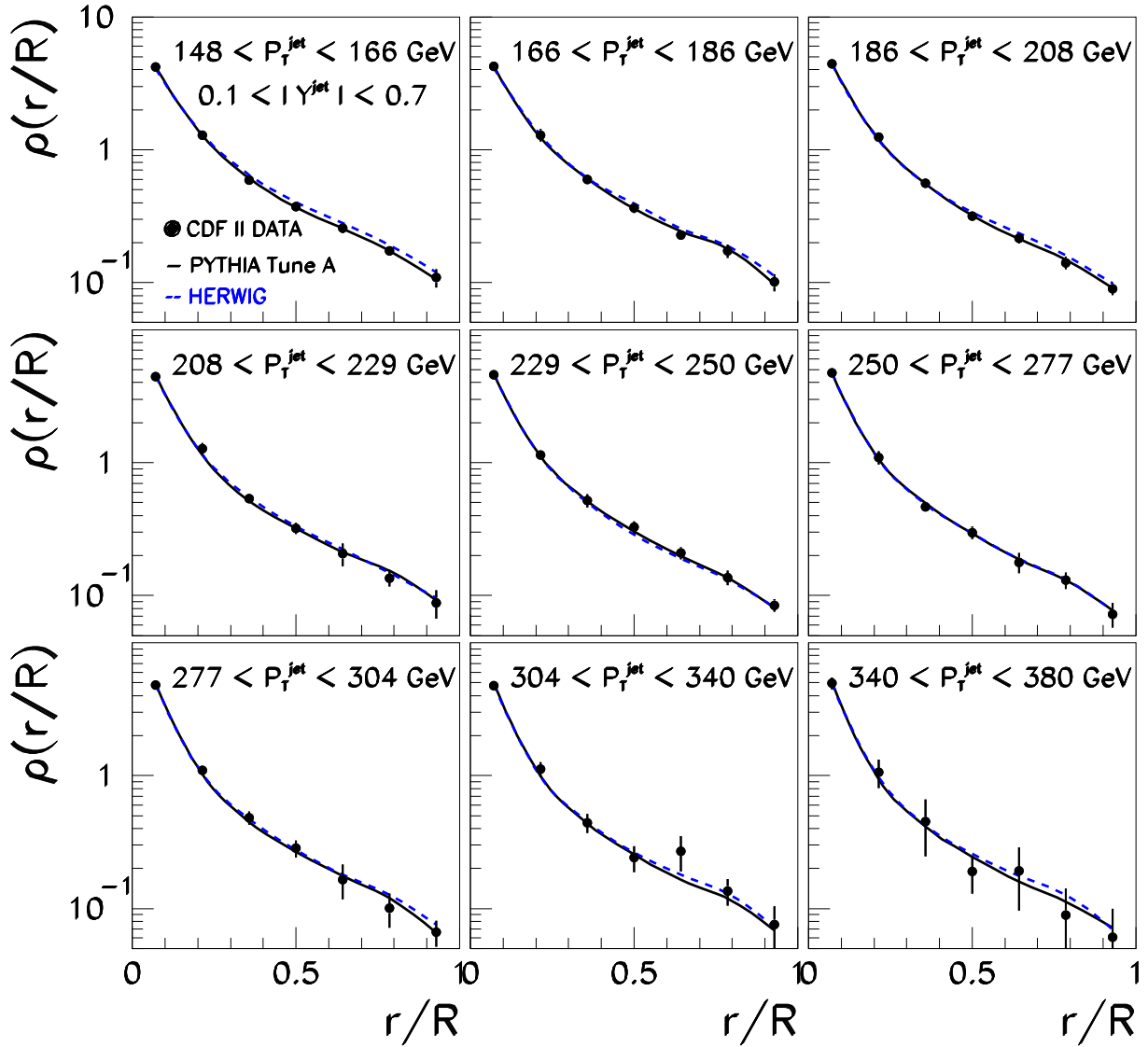


FIG. 2: The measured differential jet shape, $\rho(r/R)$, in inclusive jet production for jets with $0.1 < |Y^{\text{jet}}| < 0.7$ and $148 \text{ GeV} < P_T^{\text{jet}} < 380 \text{ GeV}$, is shown in different P_T^{jet} regions (black dots). Error bars indicate the statistical and systematic uncertainties added in quadrature. The predictions of PYTHIA-Tune A (solid lines) and HERWIG (dashed lines) are shown for comparison.

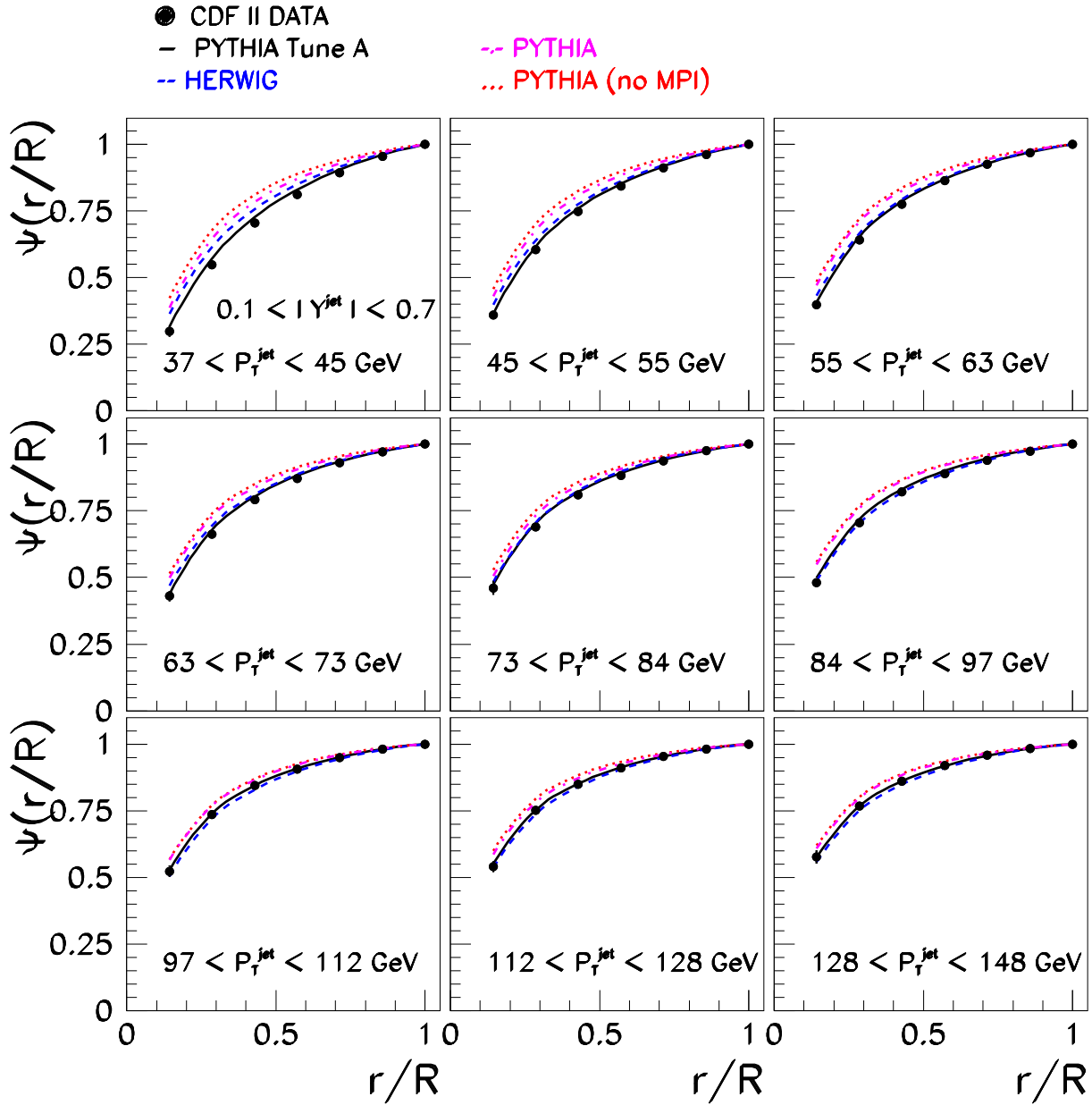


FIG. 3: The measured integrated jet shape, $\Psi(r/R)$, in inclusive jet production for jets with $0.1 < |Y^{\text{jet}}| < 0.7$ and $37 \text{ GeV} < P_T^{\text{jet}} < 148 \text{ GeV}$, is shown in different P_T^{jet} regions. Error bars indicate the statistical and systematic uncertainties added in quadrature. The predictions of PYTHIA-Tune A (solid lines), PYTHIA (dashed-dotted lines), PYTHIA-(no MPI) (dotted lines) and HERWIG (dashed lines) are shown for comparison.

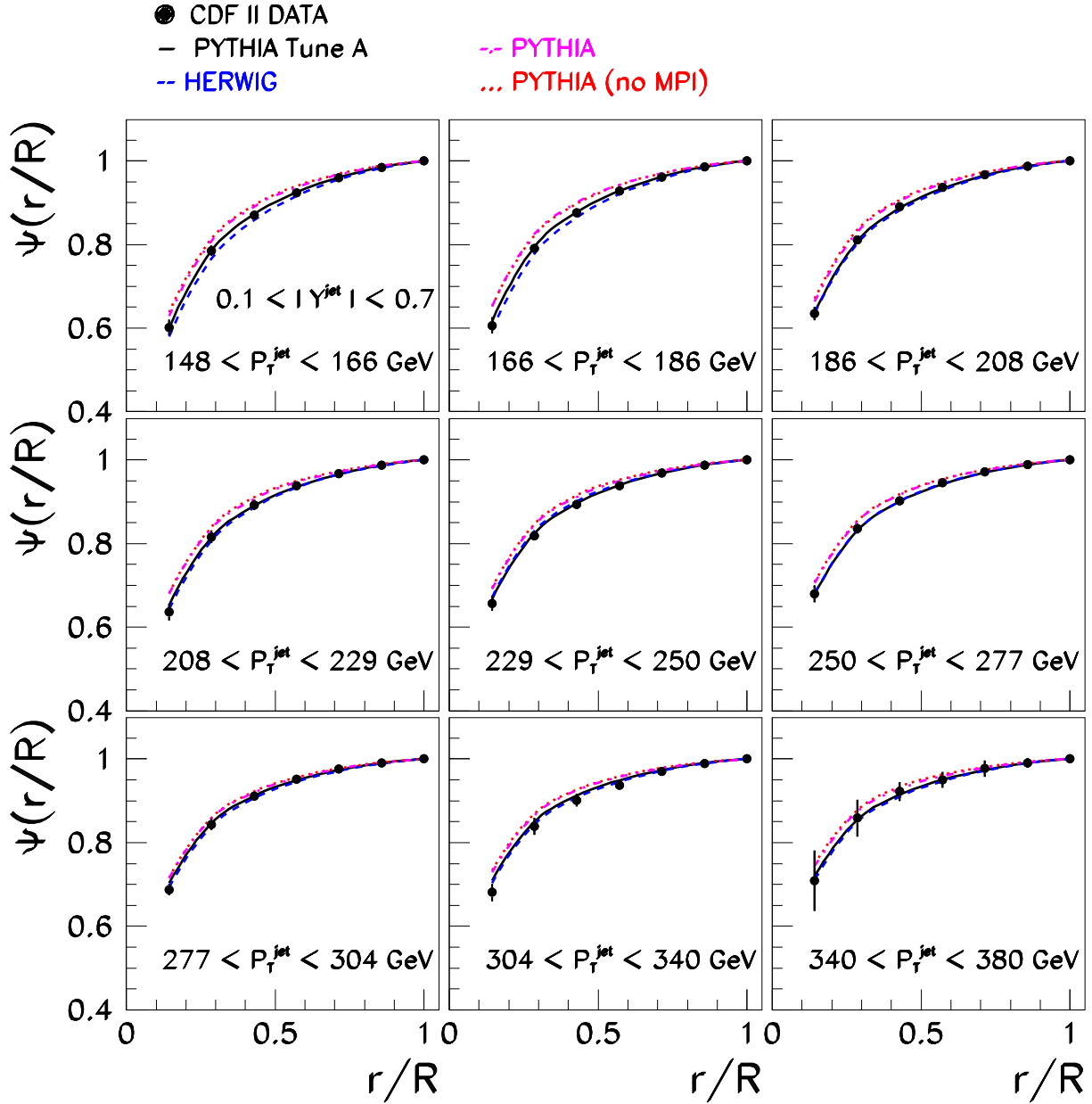


FIG. 4: The measured integrated jet shape, $\Psi(r/R)$, in inclusive jet production for jets with $0.1 < |Y^{\text{jet}}| < 0.7$ and $148 \text{ GeV} < P_T^{\text{jet}} < 380 \text{ GeV}$, is shown in different P_T^{jet} regions. Error bars indicate the statistical and systematic uncertainties added in quadrature. The predictions of PYTHIA-Tune A (solid lines), PYTHIA (dashed-dotted lines), PYTHIA-(no MPI) (dotted lines) and HERWIG (dashed lines) are shown for comparison.

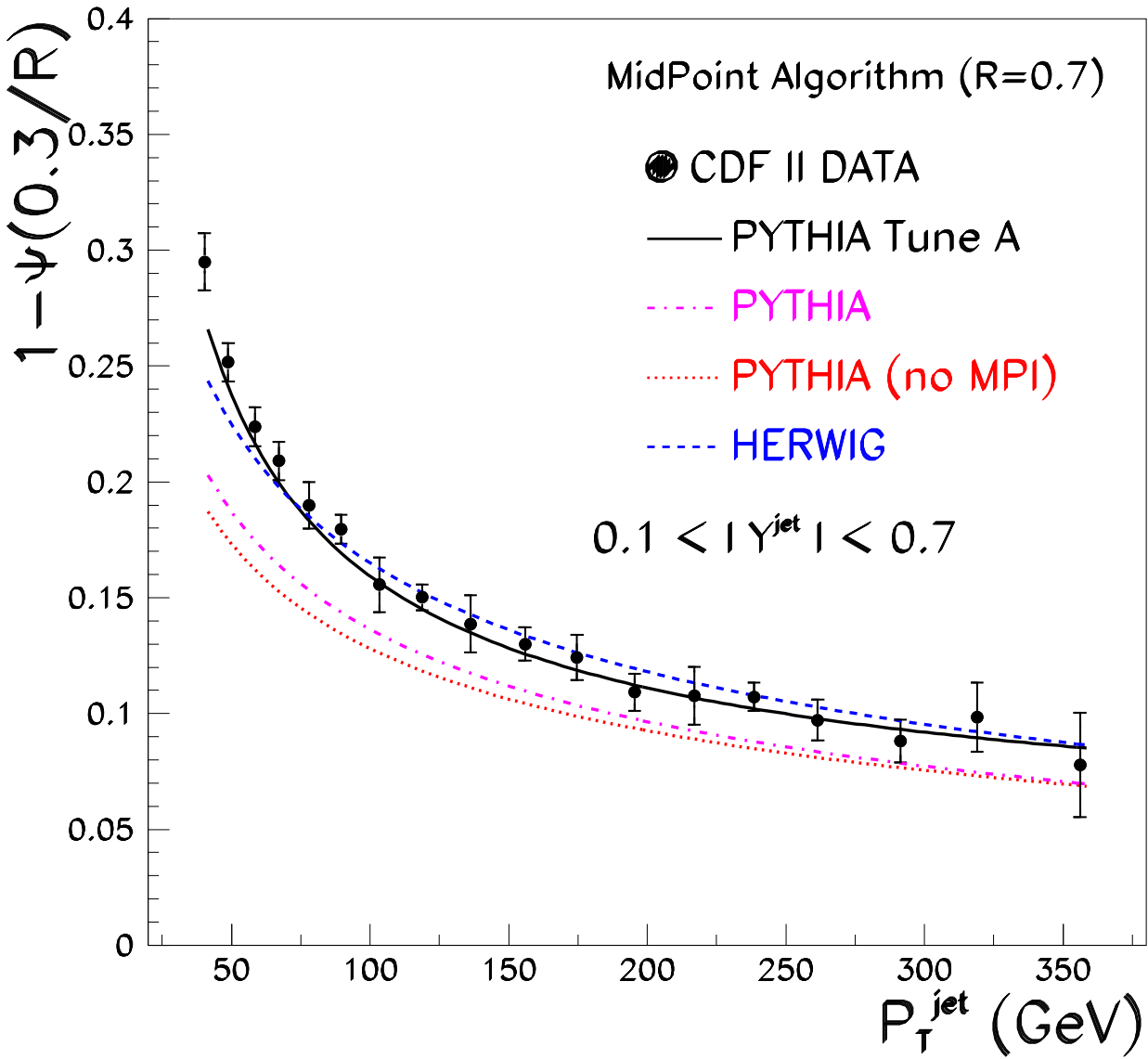


FIG. 5: The measured integrated jet shape, $1 - \Psi(0.3/R)$, as a function of P_T^{jet} for jets with $0.1 < |Y^{\text{jet}}| < 0.7$ and $37 \text{ GeV} < P_T^{\text{jet}} < 380 \text{ GeV}$. Error bars indicate the statistical and systematic uncertainties added in quadrature. The predictions of PYTHIA-Tune A (solid line), PYTHIA (dashed-dotted line), PYTHIA-(no MPI) (dotted line) and HERWIG (dashed line) are shown for comparison.

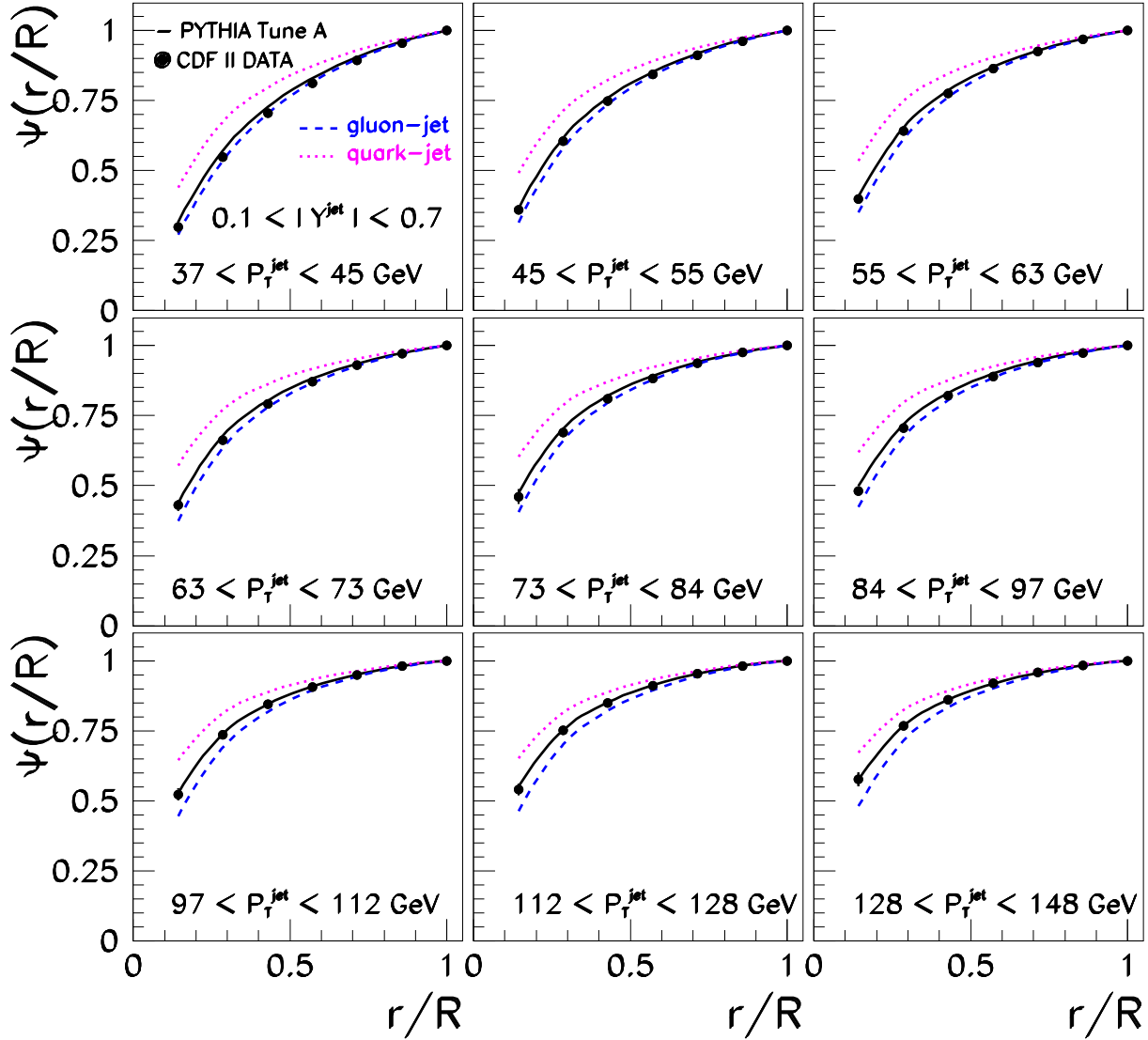


FIG. 6: The measured integrated jet shape, $\Psi(r/R)$, in inclusive jet production for jets with $0.1 < |Y^{\text{jet}}| < 0.7$ and $37 \text{ GeV} < P_T^{\text{jet}} < 148 \text{ GeV}$, is shown in different P_T^{jet} regions. Error bars indicate the statistical and systematic uncertainties added in quadrature. The predictions of PYTHIA-Tune A (solid lines) and the separated contributions from quark-initiated jets (dotted lines) and gluon-initiated jets (dashed lines) are shown for comparison.

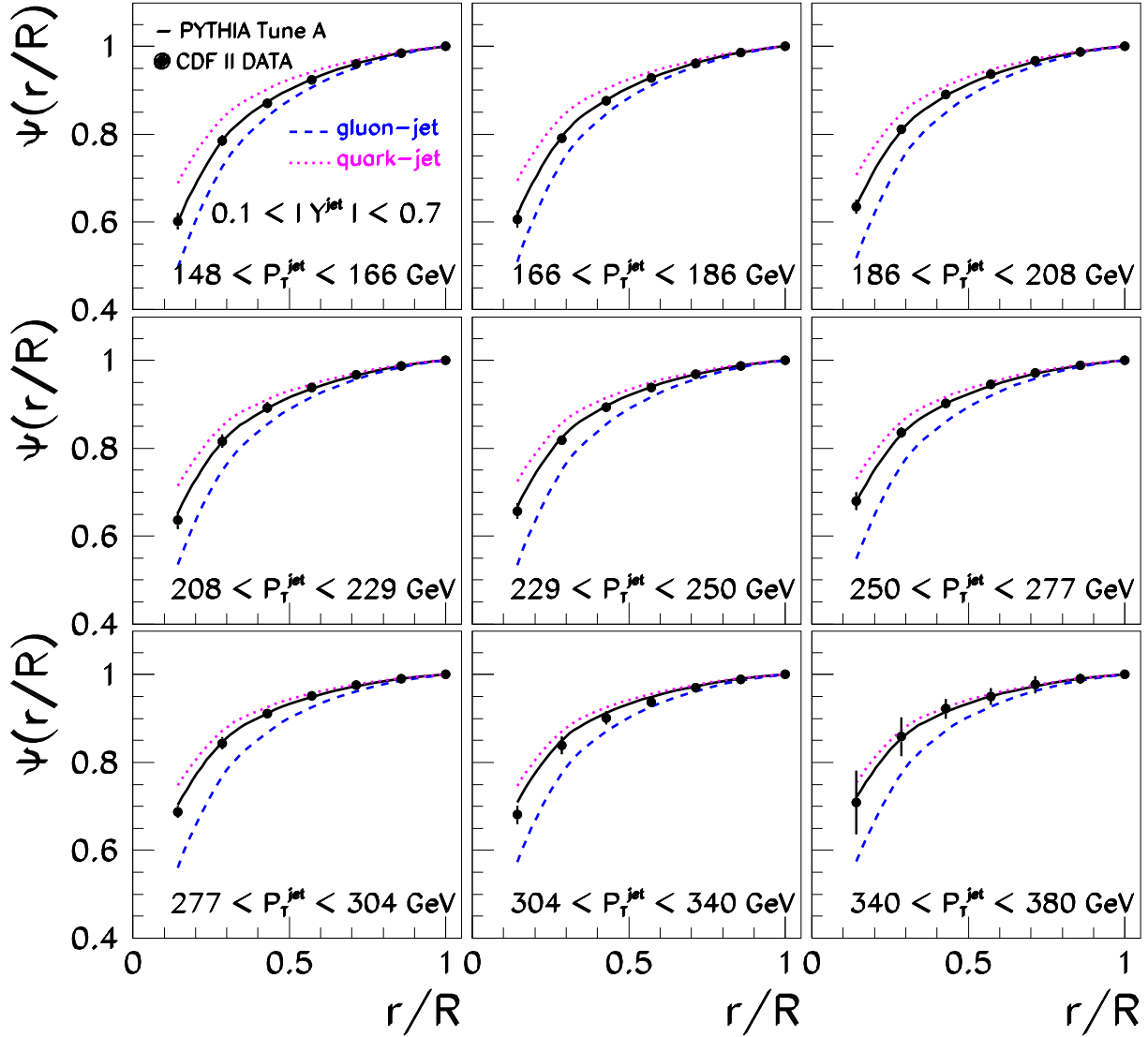


FIG. 7: The measured integrated jet shape, $\Psi(r/R)$, in inclusive jet production for jets with $0.1 < |Y^{\text{jet}}| < 0.7$ and $148 \text{ GeV} < P_T^{\text{jet}} < 380 \text{ GeV}$, is shown in different P_T^{jet} regions. Error bars indicate the statistical and systematic uncertainties added in quadrature. The predictions of PYTHIA-Tune A (solid lines) and the separated contributions from quark-initiated jets (dotted lines) and gluon-initiated jets (dashed lines) are shown for comparison.

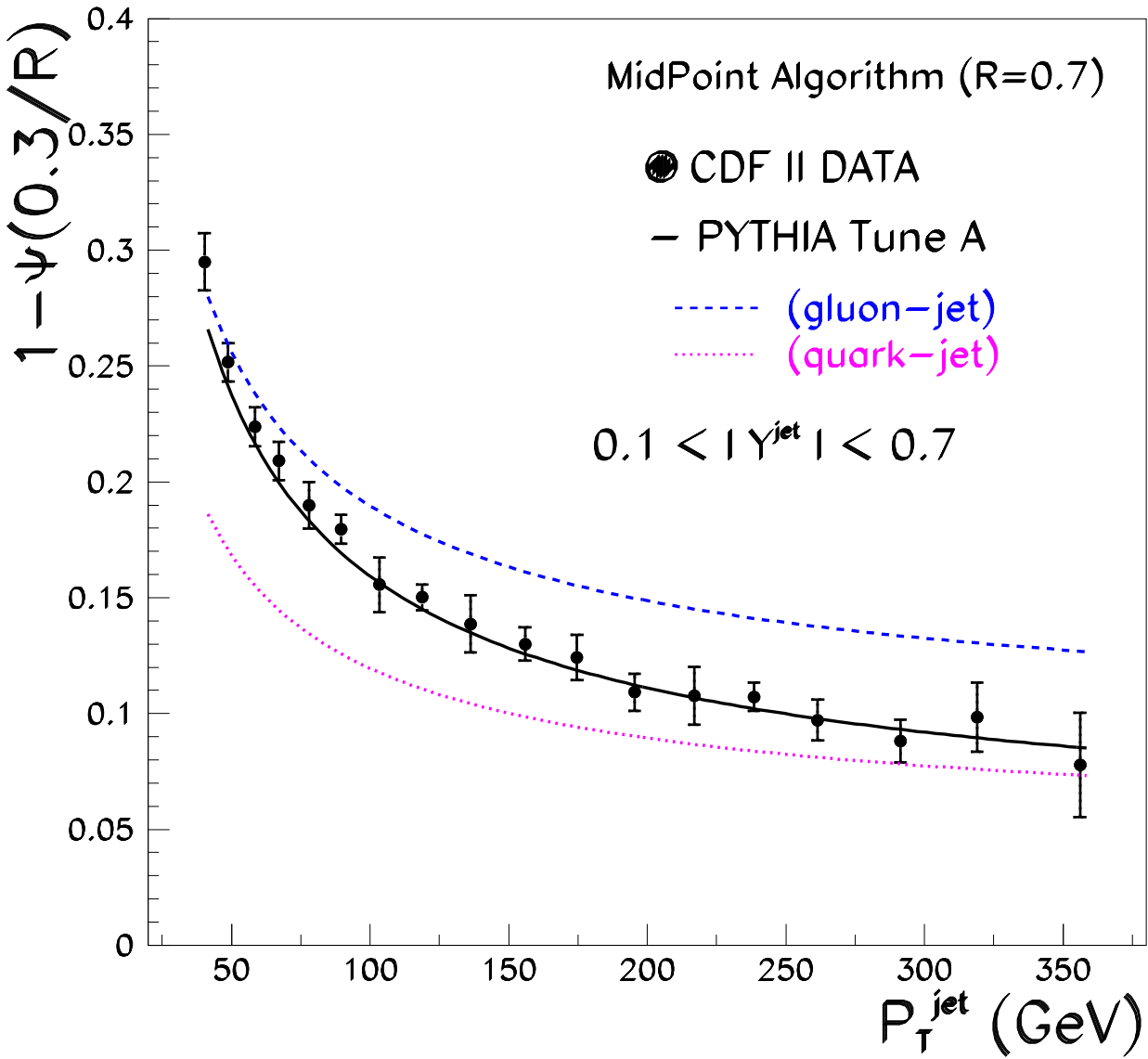


FIG. 8: The measured integrated jet shape, $1 - \Psi(0.3/R)$, as a function of P_T^{jet} for jets with $0.1 < |Y^{\text{jet}}| < 0.7$ and $37 \text{ GeV} < P_T^{\text{jet}} < 380 \text{ GeV}$. Error bars indicate the statistical and systematic uncertainties added in quadrature. The predictions of PYTHIA-Tune A (solid line) and the separated contributions from quark-initiated jets (dotted line) and gluon-initiated jets (dashed line) are shown for comparison.